

High-quality Tungsten-doped Vanadium Dioxide Thin Films Fabricated in an Extremely Low-oxygen Furnace Environment

Vishwa Krishna Rajan, Ken Araki, Robert Y. Wang, Liping Wang*

School for Engineering of Matter, Transport and Energy, Arizona State University, Tempe,
Arizona 85287, USA

* Corresponding Author. Email: Liping.Wang@asu.edu

Abstract

This work reports the fabrication and characterization of high-quality tungsten-doped vanadium dioxide ($W_xV_{1-x}O_2$, $x = 0\sim3$ at. %) by thermal oxidation of sputtered tungsten-vanadium alloyed thin films with different atomic percentages and high-temperature annealing in an extremely low oxygen atmosphere (5 to 20 ppm) along with reduction of surface over-oxides in high vacuum (1 mPa). Oxidation parameters such as temperature, time and nitrogen purging rate are first optimized for obtaining high quality undoped VO_2 thin film. Insulator-to-metal (IMT) phase transition behavior of VO_2 thin films fabricated in a low- O_2 environment is characterized with temperature dependent spectral infrared transmittance and electrical resistivity measurements, where there is 15% higher infrared transmittance change and additional 1 order change in resistivity in comparison with VO_2 thin films fabricated in a O_2 -rich environment. Grazing angle X-ray diffraction scan confirms no presence of higher oxides in the VO_2 oxidized in low- O_2 environment, which improves its quality significantly. Comprehensive studies on thermal annealing and vacuum reduction for tungsten doped VO_2 thin films are also carried out to find the optimal fabrication conditions. With the tungsten at. % measured by X-ray photoelectron spectroscopy, the optimal WVO_2 thin films fabricated through this streamlined oxidation, annealing and reduction processes in extremely low- O_2 furnace environment exhibit lowered IMT temperature at -23°C per at.% of tungsten dopants from 68°C without doping. This low-cost and scalable fabrication method could facilitate the wide development of tunable WVO_2 coatings in thermal and energy applications.

Keywords: *Vanadium dioxide, phase transition, tungsten doping, thermal annealing, spectroscopy*

1. Introduction

Thermochromic vanadium dioxide (VO_2) has attracted significant attention due to its reversible phase transition from insulating (monoclinic) phase to metallic (tetragonal) phase (IMT) at 68°C [1]. This unique behavior that leads to dramatic changes in its optical and infrared properties has found important applications in smart windows[1,2], adaptive radiative cooling [3–5], thermal rectification [6–8], and thermal camouflage [9,10]. Scalable and cost-effective fabrication of high-quality VO_2 thin films poses a significant challenge since vanadium oxides can exist in multiple oxidation states. Presence of other oxides within the film could curtail the optical properties and phase transition behaviors of any VO_2 based device in the intended temperature range. Common techniques to fabricate VO_2 thin films include chemical vapor deposition [11,12], reactive magnetron sputtering [13–15], pulsed laser deposition (PLD) [6,16–18], atomic layer deposition (ALD) [19–21], sol-gel method [22–24] and molecular beam epitaxy (MBE) [25,26]. High-quality VO_2 thin films are usually obtained in the above-mentioned techniques by precisely controlling oxygen partial pressure in a vacuum atmosphere at elevated temperatures. In addition, CVD and ALD require carefully chosen precursors that could complicate the fabrication procedures. MBE, which could yield best quality epitaxial VO_2 thin films, requires lattice-matching substrate such as sapphire and is expensive to operate.

Few works reported growth of VO_2 thin films via thermal oxidation [27–29] in a O_2 -rich atmosphere, where it suffers from excessive surface over-oxides deteriorating the phase transition performance. On the other hand, vanadium oxidation state could reduce in an extremely low- O_2 environment at high temperatures due to creation of oxygen vacancy defects in vanadium oxide crystal lattice. Several works have demonstrated the reduction of vanadium oxides from higher to lower oxidation or even back to metal vanadium at elevated temperatures in extremely low- O_2 atmosphere created by high vacuum [30–34], Ar [35–37] and N_2 [38] environment. VO_2 thin films were also obtained by reducing V_2O_5 via reactive sputtering [13], sol-gel [34] and PLD[18] techniques at similar temperature and low- O_2 atmosphere conditions.

As much as it is important to control the stoichiometry of VO_2 thin films, it is also crucial to lower its phase transition temperature for room-temperature or space applications. Doping with metal ions such as Mg [39,40], Nb [41–43], Mo [42,43] and W [44,45] is widely used since it distorts V-V dimer in the monoclinic phase thereby altering the crystal structure. For instance, introducing W atoms into VO_2 crystal lattice could lower the phase transition temperature by 15

to 25°C per at.% [44–47]. Applications such as radiative cooling [48] and spacecraft thermal control [6,49] require phase transition temperature near room temperature where >2 at.% of tungsten doping is necessary. Diffusion of tungsten atoms within the VO₂ lattice is crucial for lowering transition temperature, which could be achieved by high-temperature annealing [50–52]. While tungsten-doped VO₂ films (WVO₂) could be fabricated via ALD [46], PLD [53] and sol-gel methods [54], there is an urgent need for a more cost-effective and scalable approach for fabricating high-quality tungsten-doped VO₂ thin films.

This work aims to demonstrate the low-cost fabrication and characterization of high-quality WVO₂ thin films grown in extremely low-O₂ furnace environment from subsequent sputtering, oxidation, annealing, and vacuum reduction processes. Tungsten-vanadium alloyed thin films of different doping levels are sputtered on the 2-inch undoped silicon (UDSi) and quartz wafers. Effects of oxidation temperature, time and nitrogen gas purging rate are studied to find the optimal oxidation conditions for undoped VO₂ thin films. Temperature-dependent infrared transmittance and electrical resistivity measurements are performed to characterize the phase transition behaviors in comparison to the VO₂ film grown in O₂-rich environment. X-ray diffraction (XRD) is conducted to study the vanadium oxide states grown in both low-O₂ and O₂-rich furnace conditions. Comprehensive studies on the annealing temperature and vacuum reduction time are also carried out for WVO₂ of different doping levels. Finally, the IMT behaviors of optimally grown WVO₂ thin films are characterized with doping levels measured by X-ray photoelectron spectroscopy (XPS).

2. Methods

Figure 1 depicts the fabrication flowchart of undoped and tungsten-doped VO₂ thin films in extremely low-O₂ furnace environment as well as materials characterizations for film compositions and IMT behaviors. About 25-nm-thick vanadium or tungsten-vanadium thin films are first sputtered onto 280-μm-thick double-side polished infrared-transparent UDSi wafers in 2-inch diameter (resistivity $\rho > 10,000 \Omega \cdot \text{cm}$, orientation <100>, University Wafers Inc.). Vanadium thin film is then oxidized into high-quality VO₂ thin film in an extremely low-oxygen furnace environment by purging with N₂ gas at a proper flowrate, while tungsten-vanadium films are additionally annealed at higher temperatures after low-O₂ oxidation followed by surface reduction of over-oxides in high vacuum to obtain high-quality tungsten-doped VO₂ thin films. XRD scans

are conducted to study the oxide states and crystallinity of undoped VO_2 films, while XPS characterization is carried out to determine the tungsten doping levels within the tungsten-doped VO_2 thin films. Temperature-dependent infrared transmittance and electrical resistivity measurements are performed to reveal the IMT behaviors of undoped and tungsten-doped VO_2 thin films optimally grown in the low- O_2 furnace environment.

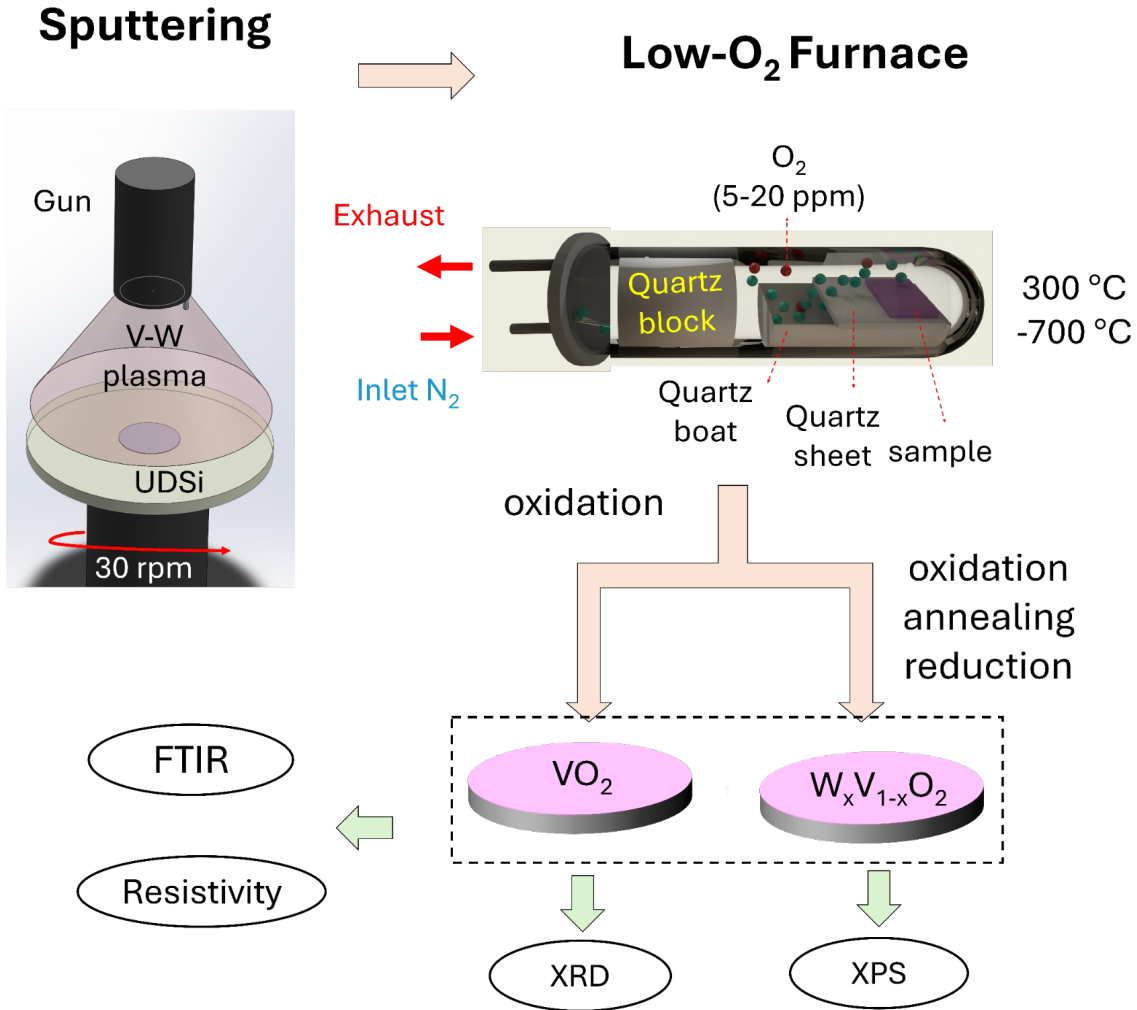


Figure 1. Flowchart to fabricate and characterize high-quality undoped and tungsten-doped VO_2 thin films thermally grown in extremely low- O_2 environment.

2.1 Sputtering of metal films

Vanadium or tungsten-vanadium thin films are sputtered onto 2-inch UDSi substrates from pure vanadium (99.99 % purity, Kurt J. Lesker) or tungsten-vanadium alloy sputter targets with ~1, ~2, ~3 at.% of tungsten (± 0.5 at.%, 99.9% purity, Stanford Advanced Materials). Once the sputtering chamber is pumped down to the base pressure of 5×10^{-6} Torr, argon gas is introduced

to maintain the chamber pressure constantly at 4 mTorr throughout the entire deposition. Magnetron gun is then turned on by a DC power supply at about 120 W to sputter the target, while the deposition rate is measured by the crystal monitor after calibration. To preclean the target and achieve a stable deposition rate, the plasma is kept on for 10 minutes with the substrate shutter closed. Once a stable deposition rate of 1.0 Å/s is reached, substrate shutter is opened to allow the deposition onto the UDSi wafers. The platen is rotated at 30 rpm throughout the entire process for the uniform deposition of the thin films. The substrate shutter is closed once the thickness from the crystal monitor reads 250 Å. The gun power is then turned off and the sample is allowed to cool down for at least 10 minutes before the chamber is vented to atmosphere.

2.2 Low-O₂ furnace setup

A hybrid furnace made of a single-ended quartz tube of 50-mm diameter inserted into a 4-inch cubic muffle furnace (KSL1100XSH, MTI Corporation) with N₂ gas purging and vacuum pumping is used to create the extremely low-O₂ environment (5~20 ppm) for oxidation, annealing and surface reduction to grow high-quality undoped and tungsten-doped VO₂ thin films. The furnace temperature ranges from 200°C to 1000°C with accuracy of $\pm 1^\circ\text{C}$ with precise proportional-integral-derivative (PID) control. The quartz tube is equipped with a flange where N₂ gas (99.99 % purity) is introduced at a few psia with its flowrate controlled by a rotameter (SKUW-493607, Aalborg Instruments) between 0.5 to 4.8 liter per minute (lpm) with 0.1 lpm resolution. The exhaust gas exiting the quartz tube passes through a trace oxygen sensor (TO2-1x, Southland Sensing Ltd) which could detect O₂ concentration from 0.01 ppm up to 25% recorded by an oxygen analyzer every 4 seconds during the process. To facilitate the surface reduction, a turbomolecular vacuum pump (Hicube 80, Pfeiffer Vacuum) is also connected to the exhaust, which could bring down the quartz tube to 1 mPa with inlet closed. Sputtered metal thin film samples are placed on a quartz sheet on top of a quartz boat sitting around one inch away from the end of the quartz tube where uniform temperature exists. A complete furnace process for growing tungsten-doped VO₂ thin films includes five stages of heating, oxidation, annealing, reduction, and cooling at different furnace temperatures and duration, which are programmed via the furnace temperature controller for a streamlined process. The photo of the furnace and schematic describing the gas lines is shown in section S1 of Supplemental Information.

2.3 Temperature-dependent infrared spectral measurements

Spectral infrared transmittance of undoped and tungsten-doped VO₂ thin films on UDSi wafers is measured between 2 to 20 μm in a wide temperature range between -30°C and 100°C with a Fourier-transform infrared (FTIR) spectrometer (Nicolet iS50, Thermo Fisher Scientific) at normal incidence. Samples are placed on a home-built temperature stage made of a copper sample holder with an 8-mm aperture, a Peltier element (TR060-6.5-40-03LS, Coherent Thermal Solutions), and a water block heat sink. A K-type thermocouple is attached to the copper sample holder next to the sample with thermal paste, and a PID temperature controller (CSi8D, OMEGA Engineering) modulates the power supplied to the Peltier element such that the sample temperature is maintained at the setpoint with $\pm 1^{\circ}\text{C}$ temperature stability. For temperatures less than 5°C , the FTIR sample compartment is purged with dry N₂ gas to prevent the formation of water and ice layers on the sample surface. Spectral measurement with 32 scans at 4 cm^{-1} resolution is taken once the sample temperature reaches the setpoint for 5 mins to ensure the steady state is achieved. Temperature-dependent spectral reflectance measurements are done similarly with a custom-built temperature stage and a 10-deg specular reflection accessory (10Spec, PIKE Technology). Please see more details on the setup and validation of FTIR measurements in the Section S2 of Supplemental Information.

2.4 Temperature-dependent four-probe resistivity measurement

The temperature-dependent resistivity of the undoped and tungsten-doped VO₂ thin films on UDSi wafers is measured using a home-built four-probe setup with a similar temperature stage. Voltage-current curves are obtained at a given temperature with a source meter (2401, Keithley), and the resistivity can be obtained by $\rho(T) = C\pi S(T)t/\ln 2$ where C is the geometrical parameter, S is the slope of V-I curve and t is thickness of the sample. Resistivity is then normalized to the lowest value in the metallic phase as $\rho(T)/\rho_m$ to show the temperature effect only on the IMT behavior of WVO₂ thin films. Please see more details on the setup and validation measurements with undoped and heavily doped silicon wafers in the Section S3 of Supplemental Information.

2.5 XRD and XPS characterizations

Grazing-incidence X-ray diffraction is respectively performed at the surface and within the film by fixing the angle of incidence as 0.5° and 2° with Cu K α X-ray source. The diffraction

pattern is matched with powder diffraction databases generated with HighScore Plus software to obtain the vanadium oxide states and assess the crystallinity of optimally grown undoped VO₂ thin films. X-ray photoelectron spectroscopy (XPS) surface scans are conducted with Kratos Axis Supra+ with Al K α 1486.6 eV X-ray source. V2p elemental scans from binding energies 510.0 eV to 540.0 eV and W4f elemental scans from binding energies 30.0 eV to 50.0 eV are performed to measure the atomic concentration of W for the optimally grown W_xV_{1-x}O₂ thin films. Raw data is analyzed and fitted with CasaXPS software with Shirley algorithm utilized to draw background for both V2p and W4f elemental scans. Lorentzian asymmetric curve is used to fit the V2p, V3p and O1s peaks while Gaussian Lorentzian peaks are used to fit the peaks of W4f. XPS scans are done at the center of the films after the films are etched with 5 keV Ar⁺ ions for 5 minutes.

3. Results and Discussion

3.1 Improved VO₂ thin film quality via low-O₂ oxidation

To obtain the best quality of thermally grown undoped VO₂ thin films in low-O₂ environment, a series of furnace oxidation tests is carried out to find optimal oxidation temperature, duration, and N₂ gas flowrate. While the quality of the VO₂ thin films could be slightly affected by the heating and cooling conditions, the oxidation parameters play a much more important role (see Section S4 in the Supplemental Information for parametric study during heating stage). Therefore, the heating ramp rate is fixed at 10°C/min, while the N₂ gas at 4.5 lpm is purged through the quartz tube to minimize oxidation during both heating and cooling stages.

Effect of oxidation temperature is studied first with the oxidation time fixed at 3 hours and N₂ gas flowrate of 1.0 lpm during oxidation. Figure 2(a) shows the infrared spectral transmittance measured at 25°C for the insulating phase and at 90°C for the metallic phase after oxidizing 25-nm vanadium thin films on UDSi substrate at different oxidation temperatures from 300°C to 700°C. The infrared transmittance is around 25% with little changes between 25°C and 90°C measurements after 300°C oxidation, suggesting that the temperature is not high enough to oxidize most of the vanadium film. With the oxidation temperature increases to 400°C, typical VO₂ phase transition is observed after the oxidation with the transmittance in the insulating phase around 53% and that in the metallic phase around 20%, confirming that vanadium film is fully oxidized. Note that the major transmittance dip around 16.6 μ m wavelength is associated with silicon phonon absorption from the UDSi substrate. Noticeably, there is a couple of minor peaks around 10 μ m

wavelength possibly due to stretching modes of vanadium oxides also observed by others [13,55][56]. With 500°C oxidation, similar typical VO₂ phase transition is also observed with slightly enhanced near-infrared transparency in the insulating phase and slightly lowered infrared transmittance in the metallic phase by 2%, indicating optimal oxidation temperature of 500°C to obtain largest transmittance change upon VO₂ IMT. When the oxidation temperature is further increased to 600°C, the film exhibits much higher transmittance reaching 40% in its metallic phase as most of the film is over-oxidized into higher vanadium oxides such as V₂O₅. Finally, with 700°C oxidation the film loses the phase transition behavior completely with almost the same high transmittance of 53% measured at both 25°C and 90°C as it is over-oxidized entirely. Note that all the oxidation tests are done in extremely low-O₂ environment as shown by the O₂ ppm level in Figure 2(b). The O₂ concentration drops down to 5 ppm at the end of heating stage with 4.5 lpm N₂ purging, then it stays around 12~18 ppm with 1.0 lpm N₂ purging during the entire oxidation stage, and finally it drops to 5 ppm again with 4.5 lpm N₂ purging during cooling.

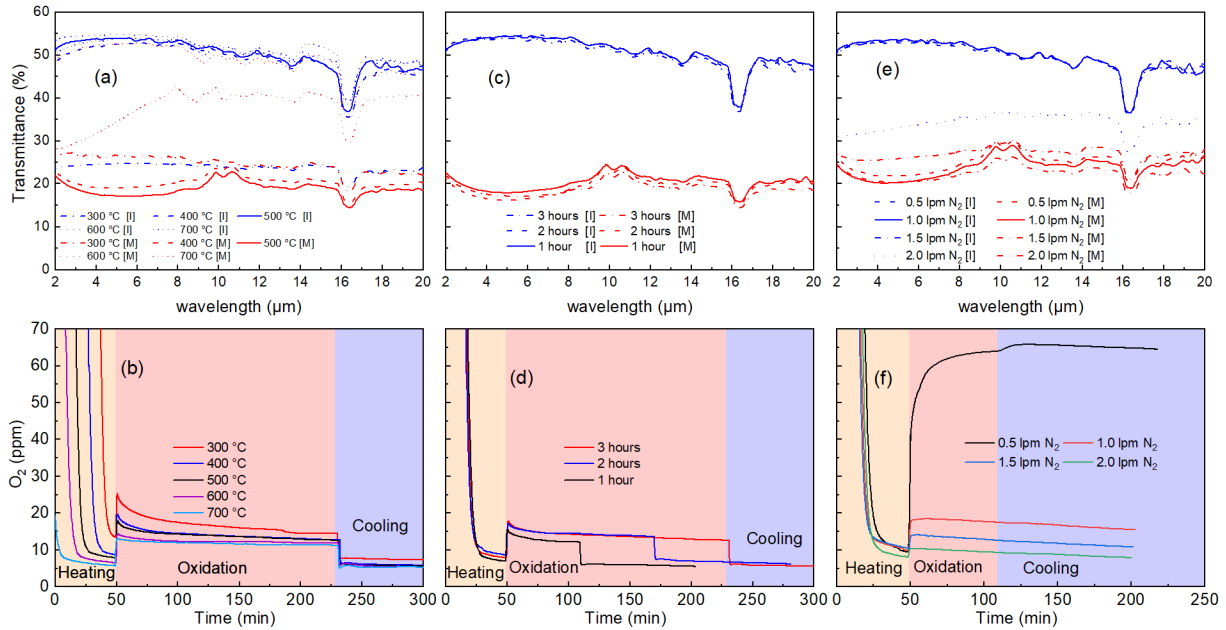


Figure 2. Low-O₂ oxidation tests for thermally growing 50-nm undoped VO₂ thin films: (a, b) effect of oxidation temperature, (c, d) effect of oxidation time, and (e, f) effect of N₂ gas flowrate, with (a, c, e) infrared spectral transmittance measured at 25°C for its insulating phase [I] and at 90°C for its metallic phase [M] along with (b, d, f) O₂ ppm level measured during each test.

With 500°C temperature and 1.0 lpm N₂ purging flowrate during oxidation, several 25-nm vanadium films of about 0.5 inch² in size are oxidized for different durations of 1, 2 and 3 hours.

As shown in Figure 2(c) and 2(d) all three films are oxidized consistently in ~ 15 ppm O_2 environment with the same typical VO_2 IMT behavior in infrared transmittance. This confirms that 1 hour oxidation time is sufficient to achieve optimal oxidation, and more importantly that, excessive oxidation time will not over-oxidize the film in such a low- O_2 environment. This is advantageous over previous furnace growth of VO_2 thin film in O_2 -rich environment, where precise control of oxidation time is required to avoid under or over-oxidation of the film. On the other hand, it is also observed that larger samples would need longer oxidation time to get fully oxidized due to extremely low concentration of oxygen in the furnace (see Section S5 in the Supplemental Information for more details). Effect of N_2 gas flowrate which is expected to change the O_2 ppm level during oxidation is studied at last with 1-hour oxidation time and $500^\circ C$ oxidation temperature. As shown in Figure 2(e), the VO_2 films after oxidization with 0.5, 1.0 and 1.5 lpm N_2 gas flowrates exhibit almost the same infrared transmittance spectra with typical IMT behavior, while the O_2 concentration varies from 65 to 10 ppm from Figure 2(f), suggesting that high quality of VO_2 thin film can be grown within this O_2 ppm range. However, with 2 lpm N_2 gas purging, the O_2 concentration during oxidation drops below 10 ppm, and much lower infrared transmittance at its insulating phase only around 35% is observed, suggesting that the vanadium film is not completely or under oxidized at the sub-10-ppm O_2 level. Finally, $500^\circ C$, 1 lpm N_2 purging rate, and 1 hour are taken as optimal oxidation parameters for oxidizing 25-nm vanadium thin films of 0.5 inch^2 in low- O_2 furnace atmosphere into high-quality VO_2 . Note that the fabrication method is scalable as VO_2 thin films have been successfully grown on 2-inch UDSi wafer with excellent uniformity as well as on other substrate materials such as quartz (see Section S5 and S6 in the Supplemental Information for more details).

To illustrate the improved quality of VO_2 thin film grown in low- O_2 furnace atmosphere, another 25-nm vanadium film is oxidized in O_2 -rich environment (7 vol.%) at $300^\circ C$ for 4 hours following our previous furnace process [27]. Temperature-dependent infrared transmittance of both VO_2 thin films is measured from $30^\circ C$ to $95^\circ C$ at $5^\circ C$ intervals outside the phase transition region and at $2^\circ C$ intervals within the phase transition (see Section S7 in the Supplemental Information). Figure 3(a) shows the heating/cooling curves of infrared transmittance at $8\text{ }\mu m$ wavelength of both 50-nm VO_2 thin films. Upon IMT phase change, the VO_2 thin film grown in low- O_2 condition achieves much larger transmittance change of 37%, while VO_2 grown in O_2 -rich environment could only achieve 8% change in transmittance. The IMT behavior is also further

compared on the transmittance derivative with respect to temperature ($d\tau/dT$) for both VO₂ thin films as shown in Figure 3(b) upon heating or cooling. The VO₂ thin film grown in low-O₂ environment exhibits up to 4% transmittance decrease per 1°C temperature change, while that grown in O₂-rich environment could only change transmission by less than 0.5% per 1°C with IMT phase transition shifted slightly to lower temperatures along with wider thermal hysteresis between heating and cooling. Temperature-dependent electrical resistivity is also measured for the IMT behaviors of both VO₂ thin films. As shown in Figure 3(c), the resistivity of the VO₂ thin film grown in low-O₂ condition exhibits 60 folds change upon IMT, while that of VO₂ thin film grown in O₂-rich environment only changes by 3 times. The resistivity derivatives with respect to temperature $d\log_{10}(\rho/\rho_m)/dT$ upon heating and cooling in Figure 3(d) presents similar behavior as the transmittance derivatives, confirming much improved VO₂ thin film quality with much sharper phase transition grown in low-O₂ condition.

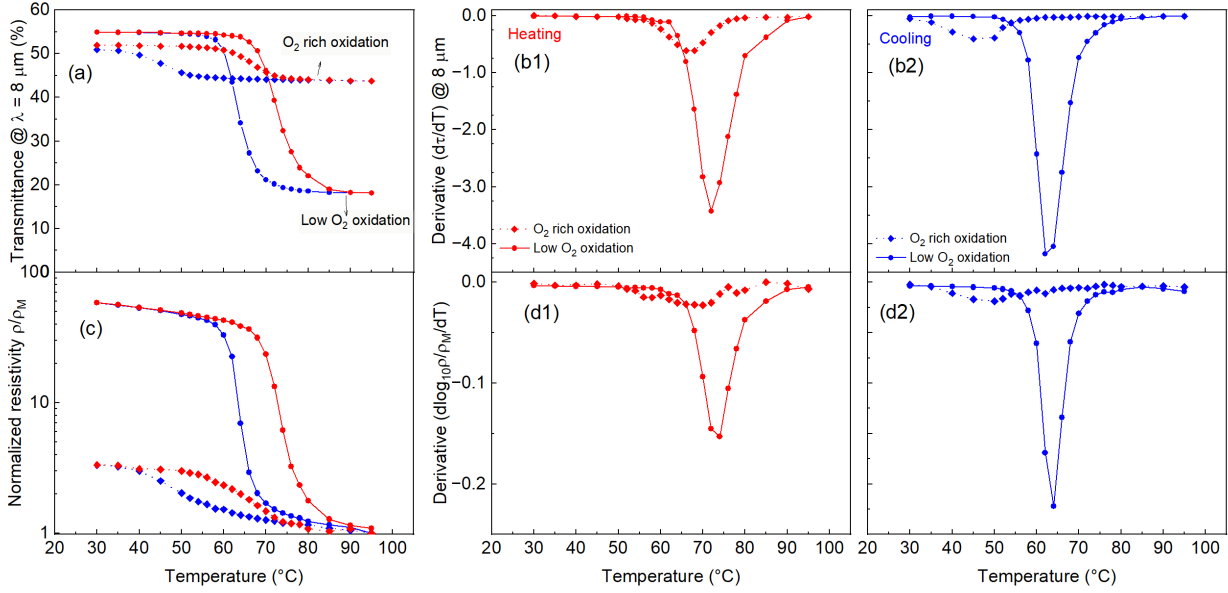


Figure 3. Insulator-to-metal transition behaviors of 50-nm VO₂ thin films thermally grown in O₂-rich and low-O₂ furnace environment with (a) temperature-dependent infrared transmittance at 8 mm wavelength and (b) its derivative with respect to temperature upon heating and cooling, as well as (c) temperature-dependent electrical resistivity normalized to the lowest value in metallic phase and (d) its derivative with respect to temperature upon heating and cooling.

It is hypothesized that, the degraded quality of VO₂ thin film grown in O₂-rich furnace environment is associated with over-oxides such as V₂O₅ formed at the film surface in the presence of high oxygen concentration, which is precisely controlled in low-O₂ environment with N₂ gas

purging and trace O₂ monitoring such that pristine VO₂ is obtained with superior IMT properties. This is confirmed by the grazing-incidence XRD scans for vanadium oxide states and phases in both VO₂ thin films grown in O₂-rich and low-O₂ furnace environment. As shown in Figure 4(a) at the film surfaces (incidence angle $\omega = 0.5^\circ$), presence of over-oxides V₂O₅ ($2\theta = 20.3^\circ, 21.7^\circ, 37.0^\circ, 50.9^\circ$) and V₄O₉ ($2\theta = 24.4^\circ$) without VO₂ is observed for VO₂ oxidized in O₂-rich atmosphere, whereas only VO₂ ($2\theta = 28.0^\circ, 40.0^\circ, 55.8^\circ, 57.8^\circ$) without any over-oxides are present for VO₂ grown in low-O₂ environment. While VO₂ and fewer over-oxides are observed within the film (incidence angle $\omega = 2^\circ$) in Figure 4(b), the existence of the over-oxides grown in O₂-rich atmosphere is undoubtedly responsible for the deterioration of VO₂ infrared properties especially in the metallic phase and its phase transition behavior. As it is clearly demonstrated here, with thermal oxidation in well-controlled low-O₂ environment, pristine VO₂ is formed at and within the film with exceptional infrared and phase-transition properties.

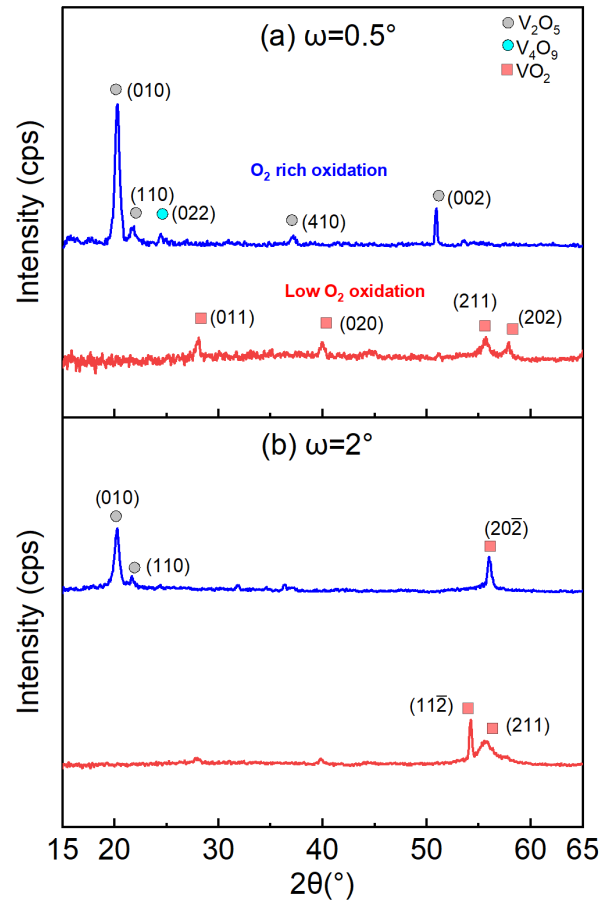


Figure 4. Grazing-incidence XRD scans for 50-nm VO₂ thin films thermally grown in O₂-rich and low-O₂ furnace environment: (a) at the surface, and (b) within the film.

3.2 Growth of tungsten-doped VO₂ thin films with thermal annealing and surface reduction

Three 25-nm tungsten-vanadium thin films sputtered from alloy targets of different tungsten doping levels are also fully oxidized in the low-O₂ furnace environment at 500°C with 1 lpm N₂ purging. However, as shown in our previous work [50] and similar works by others [51,52], thermal annealing at a higher temperature is required to fully diffuse the tungsten dopants into VO₂ crystal lattice to effectively lower the phase transition temperature. On the other hand, higher temperature would also lead to excessive over-oxidation as shown in Fig. 2(a). While a much higher N₂ purging rate could slightly mitigate the over-oxidation during annealing, the cold N₂ gas actually decreases the sample temperature which adversely results in insufficient annealing for highly doped WVO₂ films. Therefore, a slightly increased N₂ purging rate of 1.5 lpm is used during high-temperature annealing, followed by high vacuum process of 1 mPa at 450°C to reduce the surface over-oxides. A comprehensive study is carried out to find the optimal annealing temperature and optimal reduction time for the WVO₂ thin films.

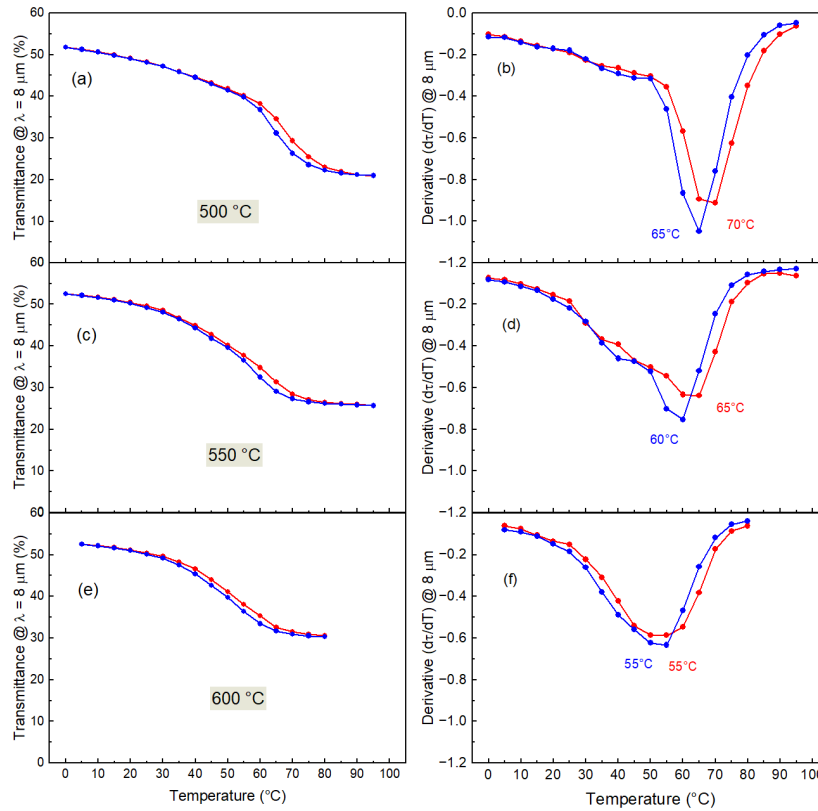


Figure 5. Annealing temperature study for ~1 at.% WVO₂: (a c, e) heating and cooling curves from infrared transmittance at 8 μm wavelength and (b, d, f) corresponding derivatives with respect to temperature for samples annealed at (a, b) 500°C, (c, d) 550°C, and (e, f) 600°C.

Figure 5 shows the annealing temperature effect for ~ 1 at.% WVO_2 thin film in terms of infrared transmittance at $8\ \mu\text{m}$ wavelength upon heating and cooling as well as its corresponding derivative. Increasing the annealing temperature from 500°C to 550°C , the IMT midpoint (i.e., temperature at which maximum derivative exists) shifts from 70°C to 65°C during heating and from 65°C to 60°C during cooling. Further increasing the annealing temperature to 600°C , the IMT midpoint is further lowered to 55°C during both heating and cooling with shortened phase transition. However, after 600°C annealing, the infrared transmittance in the metallic phase measured at 95°C is increased with a peak value approaching 35% around $10\ \mu\text{m}$ wavelength, suggesting excessive over-oxidation during the high-temperature annealing. To compensate that, the furnace is kept at 450°C and pumped down to high vacuum of 1 mPa for reducing the surface over-oxides. As shown in Fig. 6(a), vacuum reduction of 1 hour could only achieve slight improvement in lowering the short-wavelength transmittance, while reduction of 2 hours and 3 hours could bring down the entire infrared transmittance in the metallic phase effectively by nearly 10%, indicating successful reduction of surface over-oxides. This can be more clearly observed in the transmittance derivative curves in Fig. 6(b) after the ~ 1 at.% WVO_2 reduced by different amount of time in vacuum. With sufficient vacuum reduction of 2 hour, the derivative at the IMT midpoint could reach $-0.85\ \text{K}^{-1}$ compared to $-0.62\ \text{K}^{-1}$ without reduction. Reduction for longer time of 3 hours yields about the same results with 2-hour reduction.

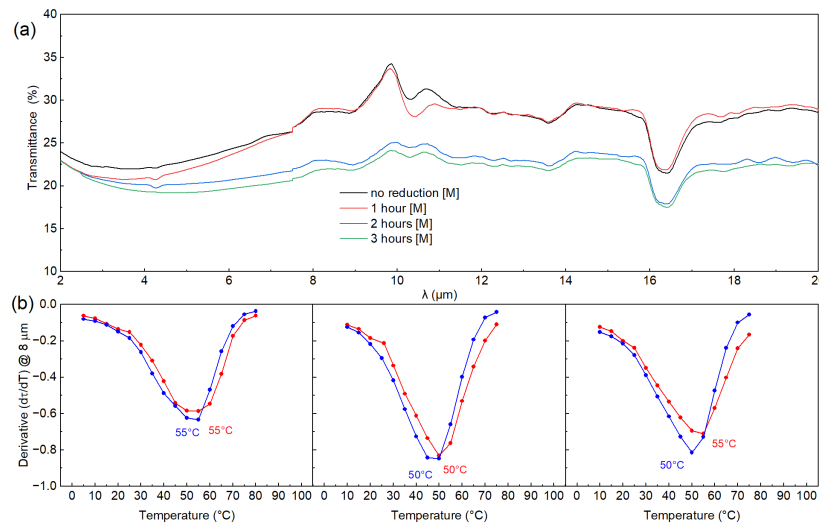


Figure 6. Reduction time study at 450°C in high vacuum (1 mPa) for ~ 1 at.% WVO_2 after 600°C and 2 hours annealing: (a) infrared transmittance of metallic phase (measured at 95°C) and (b) transmittance derivative with respect to temperature at $8\ \mu\text{m}$ wavelength upon heating and cooling without reduction and after reduction of 2 and 3 hours.

For heavily-doped WVO_2 with doping level higher than > 2 at.%, our previous study found that it requires higher temperature at least 650°C for fully annealing [50]. Therefore, ~ 2 at.% WVO_2 sample is annealed at 650°C for 2 hours followed by the vacuum reduction at 450°C for 3 hours. As shown in Fig. 7(a), the transmittance derivative at $8\ \mu\text{m}$ wavelength shows a clear dip at 35°C during heating and 30°C during cooling, indicating that the sample is fully annealed. However, the ~ 3 at.% WVO_2 sample exhibits double dips around 10°C and 55°C in the transmittance derivative after 650°C annealing, suggesting insufficient annealing, as shown in Fig. 7(b). After increasing the annealing temperature further to 675°C , a single transmission derivative dip is observed which confirms fully annealing of the ~ 3 at.% WVO_2 sample. Note that studies on annealing flowrate and reduction time for ~ 2 and ~ 3 at.% WVO_2 sample can be found in Section S9 and S10 of Supplemental Information.

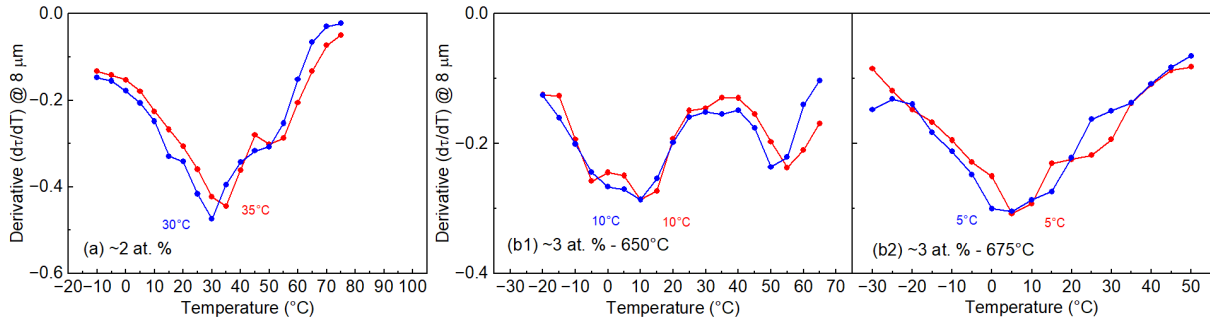


Figure 7. Thermal annealing and vacuum reduction studies in terms of transmittance derivative at $8\ \mu\text{m}$ wavelength upon heating and cooling for (a) ~ 2 at.% WVO_2 sample annealed at 650°C and (b) ~ 3 at.% WVO_2 annealed at 650°C and 675°C followed by 3-hour vacuum reduction at 450°C .

3.3 IMT behaviors of optimally grown WVO_2 thin films

After the 50-nm $\text{W}_x\text{V}_{1-x}\text{O}_2$ thin films of three different doping levels are optimally grown with the aforementioned thermal oxidation, high-temperature annealing and surface reduction processes in low- O_2 furnace environment, XPS characterizations are carried out to determine the tungsten doping levels at 3 different locations of each film after 5 mins etching with 5 keV Ar^+ ions. Figure 8 shows the V2p and W4f elemental scans of all three WVO_2 samples, from which the tungsten doping levels are determined respectively to be 1.0, 2.1 and 2.7 at.% with standard deviation of ± 0.1 , ± 0.2 and 0.2 at.% from three independent measurements.

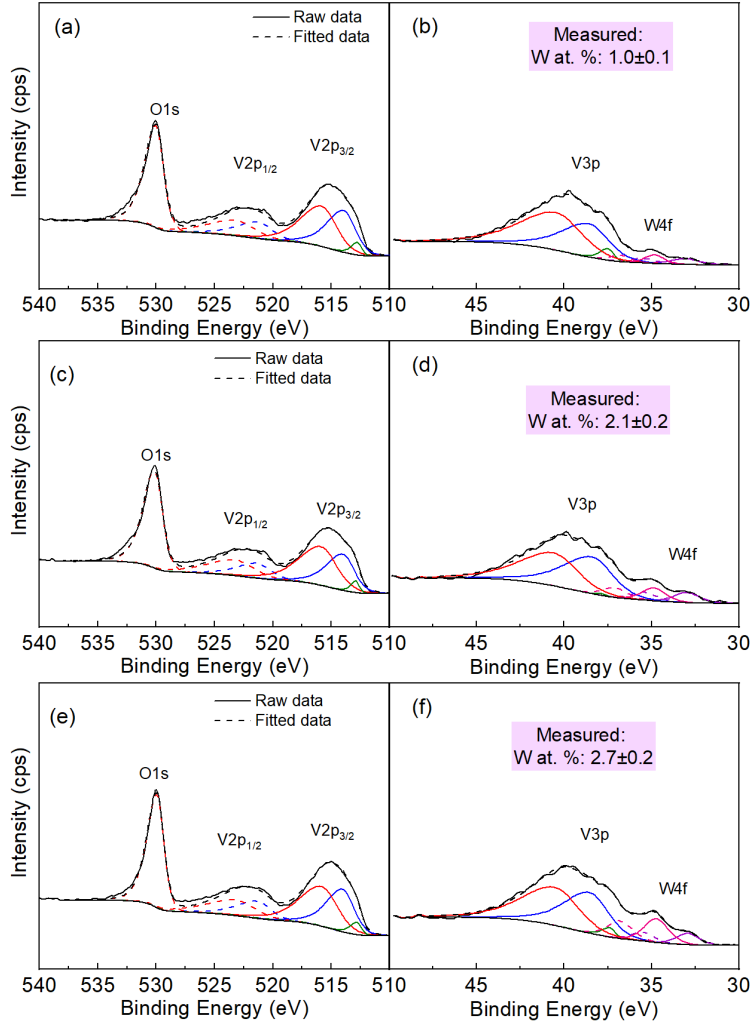


Figure 8. XPS characterization for determining tungsten doping levels of $W_xV_{1-x}O_2$ samples optimally grown in low- O_2 environment: (a) $x = 1.0$ at.%, (b) 2.1 at.%, and (c) 2.7 at.%.

Figure 9 shows the temperature-dependent infrared transmittance spectra upon heating and cooling of all four 50-nm $W_xV_{1-x}O_2$ thin films of different doping levels ($x = 0, 1.0, 2.1, 2.7$ at.%) optimally grown on UDSi wafers in low- O_2 furnace environment: (a) $x = 0$ (undoped), (b) 1.0 at.%, (c) 2.1 at.%, and (d) 2.7 at.%. The spectra are captured with every 5°C interval except for the undoped VO_2 within IMT region where 2°C interval is used. Phase transition with significant variation in transmittance is clearly observed for all WVO_2 thin films. The infrared transmittance in the insulating phase (at lowest temperature measured) drops with more tungsten doping, while the transmittance in the metallic phase (at highest temperature measured) increases slightly with pronounced peaks around $10\ \mu\text{m}$ wavelength in more heavily doped WVO_2 films due to higher temperatures required for sufficient annealing.

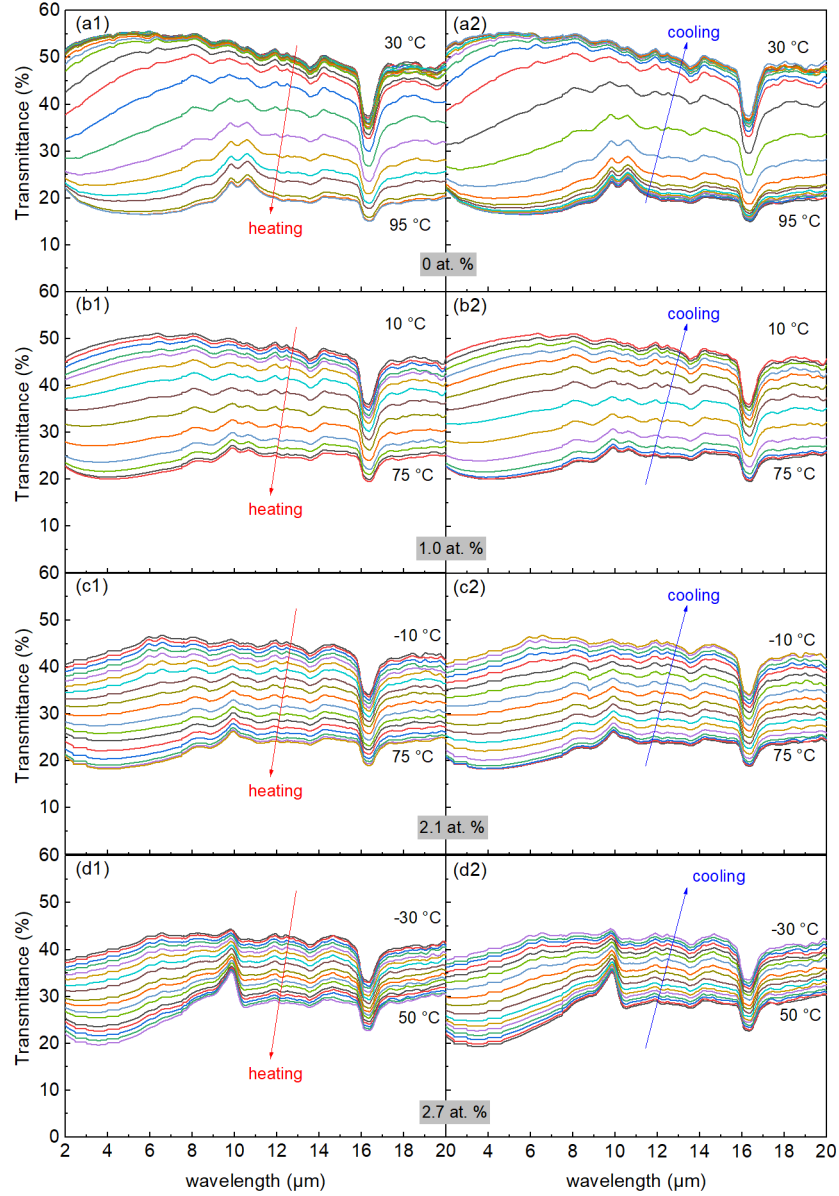


Figure 9. Temperature-dependent infrared transmittance spectra from -30°C to 95°C of all four 50-nm $\text{W}_x\text{V}_{1-x}\text{O}_2$ thin films of different doping levels optimally grown on UDSi wafers in low- O_2 furnace environment: (a) $x = 0$ (undoped), (b) 1.0 at.%, (c) 2.1 at.%, and (d) 2.7 at.%.

To better understand the IMT behaviors of all four WVO_2 films of different doping levels optimally grown in low- O_2 environment, spectral transmittance at $8\text{ }\mu\text{m}$ wavelength is plotted as a function of sample temperature upon both heating and cooling processes in Figure 10(a). Clearly, the insulator-to-metal phase transition shifts to lower temperatures with more tungsten doping. In addition, the thermal hysteresis between heating and cooling also becomes smaller from 10°C hysteresis with undoped VO_2 to almost none with 2.7 at.% tungsten doping. Figure 10(b) presents

the derivative of the infrared transmittance at 8 μm wavelength with respect to sample temperature respectively upon heating and cooling processes for all four WVO_2 thin films. The IMT derivative valley moves to lower temperatures along with smaller magnitudes with higher tungsten doping. In particular, the IMT midpoint temperatures, at which there exists the largest derivative magnitude, are 72°C, 50°C, 35°C, and 5°C upon heating and 64°C, 50°C, 30°C, and 5°C upon cooling respectively for $\text{W}_x\text{V}_{1-x}\text{O}_2$ films with doping levels of $x = 0, 1.0, 2.1$, and 2.7 at.%. Temperature-dependent electrical resistivity is also measured for these four WVO_2 thin films optimally grown in low- O_2 furnace as shown in Figure 10(c), where IMT moving to lower temperature ranges with more tungsten doping is also observed. Notably, the $\text{W}_{0.027}\text{V}_{0.973}\text{O}_2$ exhibits only 4-fold change in resistivity due to its high tungsten doping, while the films with lower doping achieve about 40 times variation in resistivity upon phase transition. Figure 10(d) presents the resistivity derivative with respect to the sample temperature for all four WVO_2 thin films, where similar behaviors with consistent IMT midpoints upon heating and cooling as infrared transmittance are observed. Finally, a linear fitting is done on the IMT midpoint temperatures and is presented in Figure 10 (e) and (f). It shows the IMT temperature decreases by 23°C upon heating or 21°C upon cooling per at.% of tungsten doping, which agree well with literature reported values [44–47].

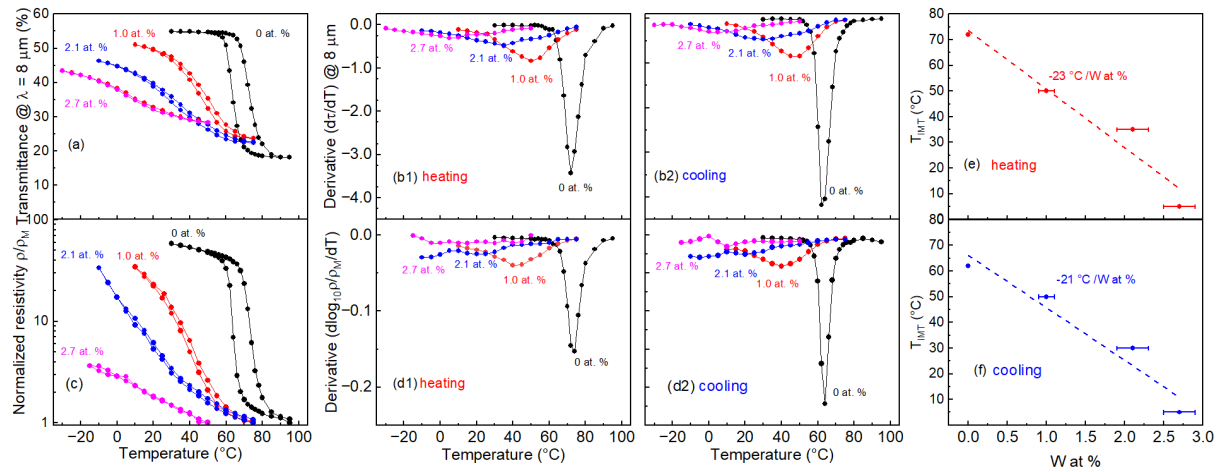


Figure 10. Insulator-to-metal transition behaviors of all four 50-nm $\text{W}_x\text{V}_{1-x}\text{O}_2$ thin films of different doping levels ($x = 0, 1.0, 2.1$ and 2.7 at.%) optimally grown on UDSi wafers via streamlined furnace oxidation, high-temperature annealing and surface reduction in low- O_2 environment: (a) temperature-dependent infrared transmittance at 8 μm wavelength and (b) its derivatives with respect to temperature upon heating and cooling; (c) temperature-dependent electrical resistivity normalized to its lowest value at metallic phase; (d) its derivatives; and transition temperature midpoint upon (e) heating and (f) cooling.

4. Conclusions

In summary, this work successfully demonstrated fabrication of high-quality WVO₂ thin films by oxidization of sputtered tungsten-vanadium alloyed thin films, high-temperature annealing, and vacuum reduction of surface over-oxides in low-O₂ furnace environment. The IMT behavior of undoped VO₂ is significantly improved compared to that oxidized in O₂-rich environment due to effective prevention of over-oxides with extremely low O₂ concentration confirmed by XRD. While surface over-oxide could be still formed at higher temperatures required for fully annealing WVO₂ thin films, vacuum reduction is implemented to improve the quality of WVO₂. Optimal oxidation, annealing and reduction conditions are determined, and the optimized WVO₂ thin films show lowered IMT temperature at the rate of $-23^{\circ}\text{C}/\text{at.}\%$ during heating and $-21^{\circ}\text{C}/\text{at.}\%$ during cooling, respectively. This cost-effective and scalable fabrication approach for high-quality WVO₂ thin films could lead to wide thermal and energy applications.

CRedit authorship contribution statement

Vishwa Krishna Rajan: Conceptualization, Data curation, Formal analysis, Investigation, Methodology, Writing-original draft, Writing-review and editing. **Ken Araki:** Data curation, Writing-review and editing. **Robert Y. Wang:** Data curation, Writing-review and editing. **Liping Wang:** Conceptualization, Formal analysis, Funding acquisition, Investigation, Methodology, Supervision, Writing-review and editing.

Acknowledgements

The work was supported by the National Science Foundation (NSF) under Grant No. CBET- 2212342. We are grateful to ASU Nanofab and Goldwater Center for using the fabrication and characterization facilities. V.K.R would like to thank ASU Graduate College and School for Engineering of Matter, Transport & Energy department for providing the financial support.

Declaration of competing interest

The authors declare that they have no known competing financial interests of personal relationships that could have appeared to influence the work reported in this paper.

References

- [1] Y. Cui, Y. Ke, C. Liu, Z. Chen, N. Wang, L. Zhang, Y. Zhou, S. Wang, Y. Gao, Y. Long, Thermochromic VO₂ for Energy-Efficient Smart Windows, *Joule* 2 (2018) 1707–1746.
- [2] C. Jiang, L. He, Q. Xuan, Y. Liao, J.G. Dai, D. Lei, Phase-change VO₂-based thermochromic smart windows, *Light Sci Appl* 13 (2024).
- [3] S. Taylor, Y. Yang, L. Wang, Vanadium dioxide based Fabry-Perot emitter for dynamic radiative cooling applications, *J Quant Spectrosc Radiat Transf* 197 (2017) 76–83.
- [4] Y. Liu, Y. Tian, X. Liu, F. Chen, A. Caratenuto, Y. Zheng, Intelligent regulation of VO₂-PDMS-driven radiative cooling, *Appl Phys Lett* 120 (2022).
- [5] S. Taylor, L. Long, R. McBurney, P. Sabbaghi, J. Chao, L. Wang, Spectrally-selective vanadium dioxide based tunable metafilm emitter for dynamic radiative cooling, *Solar Energy Materials and Solar Cells* 217 (2020).
- [6] H. Kim, K. Cheung, R.C.Y. Auyeung, D.E. Wilson, K.M. Charipar, A. Piqué, N.A. Charipar, VO₂-based switchable radiator for spacecraft thermal control, *Sci Rep* 9 (2019).
- [7] Y. Yang, S. Basu, L. Wang, Radiation-based near-field thermal rectification with phase transition materials, *Appl Phys Lett* 103 (2013).
- [8] A. Fiorino, D. Thompson, L. Zhu, R. Mittapally, S.A. Biehs, O. Bezencenet, N. El-Bondry, S. Bansropun, P. Ben-Abdallah, E. Meyhofer, P. Reddy, A Thermal Diode Based on Nanoscale Thermal Radiation, *ACS Nano* 12 (2018) 5174–5179.
- [9] L. Xiao, H. Ma, J. Liu, W. Zhao, Y. Jia, Q. Zhao, K. Liu, Y. Wu, Y. Wei, S. Fan, K. Jiang, Fast Adaptive Thermal Camouflage Based on Flexible VO₂/Graphene/CNT Thin Films, *Nano Lett* 15 (2015) 8365–8370.
- [10] D. Liu, H. Ji, R. Peng, H. Cheng, C. Zhang, Infrared chameleon-like behavior from VO₂(M) thin films prepared by transformation of metastable VO₂(B) for adaptive camouflage in both thermal atmospheric windows, *Solar Energy Materials and Solar Cells* 185 (2018) 210–217.
- [11] D. Malarde, M.J. Powell, R. Quesada-Cabrera, R.L. Wilson, C.J. Carmalt, G. Sankar, I.P. Parkin, R.G. Palgrave, Optimized Atmospheric-Pressure Chemical Vapor Deposition Thermochromic VO₂ Thin Films for Intelligent Window Applications, *ACS Omega* 2 (2017) 1040–1046.
- [12] B. Rajeswaran, A.M. Umarji, Defect engineering of VO₂ thin films synthesized by Chemical Vapor Deposition, *Mater Chem Phys* 245 (2020).
- [13] C. Wan, Z. Zhang, D. Woolf, C.M. Hessel, J. Rensberg, J.M. Hensley, Y. Xiao, A. Shahsafi, J. Salman, S. Richter, Y. Sun, M.M. Qazilbash, R. Schmidt-Grund, C. Ronning, S. Ramanathan, M.A. Kats, On the Optical Properties of Thin-Film Vanadium Dioxide from the Visible to the Far Infrared, *Ann Phys* 531 (2019).
- [14] G. Fu, A. Polity, N. Volbers, B.K. Meyer, Annealing effects on VO₂ thin films deposited by reactive sputtering, *Thin Solid Films* 515 (2006) 2519–2522.
- [15] Y.Y. Luo, L.Q. Zhu, Y.X. Zhang, S.S. Pan, S.C. Xu, M. Liu, G.H. Li, Optimization of microstructure and optical properties of VO₂ thin film prepared by reactive sputtering, *J Appl Phys* 113 (2013).

- [16] D.H. Kim, H.S. Kwok, Pulsed laser deposition of VO₂ thin films, *Appl Phys Lett* 65 (1994) 3188–3190.
- [17] S.A. Bukhari, S. Kumar, P. Kumar, S.P. Gumfekar, H.J. Chung, T. Thundat, A. Goswami, The effect of oxygen flow rate on metal–insulator transition (MIT) characteristics of vanadium dioxide (VO₂) thin films by pulsed laser deposition (PLD), *Appl Surf Sci* 529 (2020).
- [18] E.K. Barimah, A. Boontan, D.P. Steenson, G. Jose, Infrared optical properties modulation of VO₂ thin film fabricated by ultrafast pulsed laser deposition for thermochromic smart window applications, *Sci Rep* 12 (2022).
- [19] G.Y. Song, C. Oh, S. Sinha, J. Son, J. Heo, Facile Phase Control of Multivalent Vanadium Oxide Thin Films (V₂O₅ and VO₂) by Atomic Layer Deposition and Postdeposition Annealing, *ACS Appl Mater Interfaces* 9 (2017) 23909–23917.
- [20] A.M. Morsy, M.T. Barako, V. Jankovic, V.D. Wheeler, M.W. Knight, G.T. Papadakis, L.A. Sweatlock, P.W.C. Hon, M.L. Povinelli, Experimental demonstration of dynamic thermal regulation using vanadium dioxide thin films, *Sci Rep* 10 (2020).
- [21] V.P. Prasad, B. Dey, S. Bulou, T. Schenk, N. Bahlawane, Study of VO₂ thin film synthesis by atomic layer deposition, *Mater Today Chem* 12 (2019) 332–342.
- [22] Y. Ningyi, L. Jinhua, L. Chenglu, Valence reduction process from sol-gel V₂O₅ to VO₂ thin films, n.d.
- [23] B.G. Chae, H.T. Kim, S.J. Yun, B.J. Kim, Y.W. Lee, D.H. Youn, K.Y. Kang, Highly oriented VO₂ thin films prepared by sol-gel deposition, *Electrochemical and Solid-State Letters* 9 (2006).
- [24] N. Wang, S. Magdassi, D. Mandler, Y. Long, Simple sol-gel process and one-step annealing of vanadium dioxide thin films: Synthesis and thermochromic properties, *Thin Solid Films* 534 (2013) 594–598.
- [25] J.W. Tashman, J.H. Lee, H. Paik, J.A. Moyer, R. Misra, J.A. Mundy, T. Spila, T.A. Merz, J. Schubert, D.A. Muller, P. Schiffer, D.G. Schlom, Epitaxial growth of VO₂ by periodic annealing, *Appl Phys Lett* 104 (2014).
- [26] H. Paik, J.A. Moyer, T. Spila, J.W. Tashman, J.A. Mundy, E. Freeman, N. Shukla, J.M. Lapano, R. Engel-Herbert, W. Zander, J. Schubert, D.A. Muller, S. Datta, P. Schiffer, D.G. Schlom, Transport properties of ultra-thin VO₂ films on (001) TiO₂ grown by reactive molecular-beam epitaxy, *Appl Phys Lett* 107 (2015).
- [27] S. Taylor, L. Long, L. Wang, Fabrication and characterization of furnace oxidized vanadium dioxide thin films, *Thin Solid Films* 682 (2019) 29–36.
- [28] A. P, Y.S. Chauhan, A. Verma, Vanadium dioxide thin films synthesized using low thermal budget atmospheric oxidation, *Thin Solid Films* 706 (2020).
- [29] P. Guo, Z. Biegler, T. Back, A. Sarangan, Vanadium dioxide phase change thin films produced by thermal oxidation of metallic vanadium, *Thin Solid Films* 707 (2020).
- [30] Z. Zhang, F. Zuo, C. Wan, A. Dutta, J. Kim, J. Rensberg, R. Nawrodt, H.H. Park, T.J. Larrabee, X. Guan, Y. Zhou, S.M. Prokes, C. Ronning, V.M. Shalae, A. Boltasseva, M.A. Kats, S. Ramanathan, Evolution of Metallicity in Vanadium Dioxide by Creation of Oxygen Vacancies, *Phys Rev Appl* 7 (2017).

- [31] C. V. Ramana, S. Utsunomiya, R.C. Ewing, U. Becker, Formation of V₂O₃ nanocrystals by thermal reduction of V₂O₅ thin films, *Solid State Commun* 137 (2006) 645–649.
- [32] M. Heber, W. Grünert, Application of ultraviolet photoelectron spectroscopy in the surface characterization of polycrystalline oxide catalysts. 2. Depth variation of the reduction degree in the surface region of partially reduced V₂O₅, *Journal of Physical Chemistry B* 104 (2000) 5288–5297.
- [33] E. Hryha, E. Rutqvist, L. Nyborg, Stoichiometric vanadium oxides studied by XPS, in: *Surface and Interface Analysis*, 2012: pp. 1022–1025.
- [34] O. Monfort, T. Roch, L. Satrapinskyy, M. Gregor, T. Plecenik, A. Plecenik, G. Plesch, Reduction of V₂O₅ thin films deposited by aqueous sol-gel method to VO₂ (B) and investigation of its photocatalytic activity, *Appl Surf Sci* 322 (2014) 21–27.
- [35] M. Foguel, FLUX GROWTH OF V₂O₃ SINGLE CRYSTALS BY REDUCTION OF V₂O₅ IN A GRAPHITE CRUCIBLE, 1971.
- [36] C.H. Griffiths, H.K. Eastwood, Influence of stoichiometry on the metal-semiconductor transition in vanadium dioxide, *J Appl Phys* 45 (1974) 2201–2206.
- [37] M. Gotić, S. Popović, M. Ivanda, S. Musić, Sol-gel synthesis and characterization of V₂O₅ powders, *Mater Lett* 57 (2003) 3186–3192.
- [38] D.K. Manousou, S. Gardelis, M. Calamiotou, E. Syskakis, VO₂ thin films fabricated by reduction of thermal evaporated V₂O₅ under N₂ flow, *Mater Lett* 299 (2021).
- [39] S.Y. Li, N.R. Mlyuka, D. Primetzhofer, A. Hallén, G. Possnert, G.A. Niklasson, C.G. Granqvist, Bandgap widening in thermochromic Mg-doped VO₂ thin films: Quantitative data based on optical absorption, *Appl Phys Lett* 103 (2013).
- [40] N.R. Mlyuka, G.A. Niklasson, C.G. Granqvist, Mg doping of thermochromic VO₂ films enhances the optical transmittance and decreases the metal-insulator transition temperature, *Appl Phys Lett* 95 (2009).
- [41] C. Piccirillo, R. Binions, I.P. Parkin, Nb-doped VO₂ thin films prepared by aerosol-assisted chemical vapour deposition, *Eur J Inorg Chem* (2007) 4050–4055.
- [42] C. Batista, R.M. Ribeiro, V. Teixeira, Synthesis and characterization of VO₂-based thermochromic thin films for energy-efficient windows, *Nanoscale Res Lett* 6 (2011).
- [43] C.B. Greenberg, Undoped and doped VO₂ films grown from VO (OC₃H₇)₃, *Thin Solid Films* 110 (1983) 73–82.
- [44] R. Binions, C. Piccirillo, I.P. Parkin, Tungsten doped vanadium dioxide thin films prepared by atmospheric pressure chemical vapour deposition from vanadyl acetylacetonate and tungsten hexachloride, *Surf Coat Technol* 201 (2007) 9369–9372.
- [45] A. Romanyuk, R. Steiner, L. Marot, P. Oelhafen, Temperature-induced metal-semiconductor transition in W-doped VO₂ films studied by photoelectron spectroscopy, *Solar Energy Materials and Solar Cells* 91 (2007) 1831–1835.
- [46] K. Sun, C. Wheeler, J.A. Hillier, S. Ye, I. Zeimpekis, A. Urbani, N. Kalfagiannis, O.L. Muskens, C.H. de Groot, Room Temperature Phase Transition of W-Doped VO₂ by Atomic Layer Deposition on 200 mm Si Wafers and Flexible Substrates, *Adv Opt Mater* 10 (2022).
- [47] Y. Li, H. Ma, R. Shi, Y. Wu, S. Feng, Y. Fu, Y. Wei, X. Zhao, K. Dong, K. Jiang, K. Liu, X. Zhang, Wafer-Scale Transfer and Integration of Tungsten-Doped Vanadium Dioxide Films, *ACS Nano* (2025).

- [48] K. Tang, K. Dong, J. Li, M.P. Gordon, F.G. Reichertz, H. Kim, Y. Rho, Q. Wang, C.-Y. Lin, C.P. Grigoropoulos, Temperature-adaptive radiative coating for all-season household thermal regulation, *Science* (1979) 374 (2021) 1504–1509.
- [49] E. Haddad, R. V Kruzelecky, P. Murzionak, W. Jamroz, K. Tagziria, M. Chaker, B. Ledrogoff, Review of the VO₂ smart material applications with emphasis on its use for spacecraft thermal control, *Front Mater* 9 (2022) 1013848.
- [50] V.K. Rajan, J. Chao, S. Taylor, L. Wang, Lowering insulator-to-metal transition temperature of vanadium dioxide thin films via co-sputtering, furnace oxidation, and thermal annealing, *J Appl Phys* 137 (2025).
- [51] Q. Song, H. Pang, W. Gong, G. Ning, Y. Zhang, X. Cheng, Y. Lin, Enhancing phase-transition sensitivity of tungsten-doped vanadium dioxide by high temperature annealing, *Mater Lett* 161 (2015) 244–247.
- [52] J. Zou, X. Chen, L. Xiao, Phase transition performance recovery of W-doped VO₂ by annealing treatment, *Mater Res Express* 5 (2018).
- [53] S. Choi, G. Ahn, S.J. Moon, S. Lee, Tunable resistivity of correlated VO₂(A) and VO₂(B) via tungsten doping, *Sci Rep* 10 (2020).
- [54] A. V. Ivanov, A.Y. Tatarenko, A.A. Gorodetsky, O.N. Makarevich, M. Navarro-Cía, A.M. Makarevich, A.R. Kaul, A.A. Eliseev, O. V. Boytsova, Fabrication of Epitaxial W-Doped VO₂ Nanostructured Films for Terahertz Modulation Using the Solvothermal Process, *ACS Appl Nano Mater* 4 (2021) 10592–10600.
- [55] F. Guinneton, L. Sauques, J.C. Valmalette, F. Cros, J.R. Gavarri, Comparative study between nanocrystalline powder and thin film of vanadium dioxide VO₂: electrical and infrared properties, n.d.
- [56] K. Shibuya, A. Sawa, Optimization of conditions for growth of vanadium dioxide thin films on silicon by pulsed-laser deposition, *AIP Adv* 5 (2015).